High Resolution Imaging of Magnetization

D.T. Pierce, J. Unguris, and R.J. Celotta

Introduction

In 1907 Weiss postulated that a ferromagnet has many small regions or domains that are spontaneously magnetized below the Curie temperature.[1] In an unmagnetized ferromagnetic specimen the domains form so as to minimize the free energy, which includes contributions from the exchange energy, crystal and shape anisotropy energy, magnetostrictive energy, and so on. The actual size and shape of domains can only be calculated for the simplest geometries and for idealized materials. To investigate magnetic microstructure and how it determines macroscopic magnetic properties, we want to be able to see domain configurations and understand how the magnetic microstructure is changed by external influences and varying material properties. The observation of microscopic domain configurations can aid in engineering magnetic materials with desired magnetic properties.

Domains were first observed using the Bitter method in which fine magnetic particles collect on the surface of a specimen in the field gradients at domain walls.[2,3] Domains can also be observed by electron microscopy, with scanning electron microscopy,[4] or at higher resolution with transmission electron microscopy.[5] Specimens must be thinned to about 100 nm for use in the TEM. This, in turn, changes their magnetic properties. The magneto-optic Kerr effect [6] has the advantage that the signal is directly related to the magnetization of the specimen and not just to the leakage fields or internal magnetic fields as in the methods mentioned above. This technique has the disadvantage of being limited to an optical resolution of typically 1μm.

What is needed is a high resolution, domain-imaging technique in which the signal contrast is directly proportional to the magnetization. Ideally, such an imaging technique could be applied to thick specimens in order to image magnetic structures on a nonmagnetic substrate, such as a bit written on a magnetic disk, or a permalloy memory element on a silicon chip. It is the object of this article to describe such a high resolution imaging technique that has been developed over the past few years.

A New Magnetization Imaging Technique

Over the last couple decades, electron spin polarization techniques have been developed to gain insight into fundamental aspects of ferromagnetism.[7,8] A measurement of electron spin polarization is extremely valuable because the magnetization M is proportional to the net spin density $n_\uparrow - n_\downarrow$. For example, in a 3d ferromagnet such as Fe, Co, or Ni in which the orbital magnetic moment is quenched:

$$M = -\mu_B(n_\uparrow - n_\downarrow) \qquad (1)$$

The electron spin magnetic moment or Bohr magnetron is denoted as μ_B and $n_\uparrow(n_\downarrow)$ is the number of spins per unit volume parallel (antiparallel) to a particular direction. Thus, the magnetization, which derives from the preferential alignment of the spin magnetic moments in some direction, can be investigated if these electrons are ejected from the solid without change in their spin orientation and that spin orientation subsequently measured.

A few years ago we measured[9] the energy distribution of the polarization of secondary electrons emitted when a 500 eV primary energy electron beam was incident on a ferromagnetic glass. One component of the polarization vector, for example in the z direction, is defined as

$$P_z = \frac{N_\uparrow - N_\downarrow}{N_\uparrow + N_\downarrow} \qquad (2)$$

where $N_\uparrow(N_\downarrow)$ are the number of electrons with spins parallel (antiparallel to the z direction). The polarization was found to be oriented antiparallel to the magnetization direction, high in value, and highest at low energies where the most secondary electrons are emitted. Explanations of the variation of P with secondary electron energy have since been suggested.[10,11] These and subsequent measurements on single crystals[12,13] have shown that at secondary electron energies just above the low energy range where P increases, the polarization corresponds to what would be expected from a representative sampling of the valence band which for Fe, Co, and Ni corresponds to a polarization of 28%, 19%, and 5%, respectively.

While our secondary electron measurements were made on a single domain sample, they led us to consider[14] the possibility of using a finely focused high energy electron beam in a scanning electron microscope to generate the secondaries within a small domain. If the secondary electron spin polarization is measured as the SEM beam is scanned across the specimen, according to Eqs. 1 and 2, an image of the sample magnetization is obtained. We refer to this technique as scanning electron microscopy with polarization analysis or SEMPA. It has also been referred to as SEM type III magnetic contrast.[4] Indeed, the contrast can be very high. An important feature of SEMPA is that the same electrons that are detected to give the magnetization image also produce the secondary electron intensity topographic image. Hence, the physical structure and the magnetic structure of the surface are measured simultaneously but independently. It is therefore possible to directly correlate the physical structure and the magnetic structure. The spatial resolution of a magnetization image obtained with SEMPA is the same as that of a conventional topographic image and ultimately depends on the size of the SEM electron beam. Because the secondary electrons come from depths of a few nanometers, the magnetization image is very sensitive to contamination on the specimen surface, and the specimen must be cleaned and maintained in ultrahigh vacuum.

The key feature of a SEMPA instrument, which distinguishes it from an ordinary SEM, is the spin analyzer. Tra-

ditionally, spin analysis has been carried out using a Mott spin analyzer, which operates by accelerating the electron beam to 100 keV and measuring the spin-orbit-induced spatial asymmetry when the beam scatters from a gold foil.[15] In fact, the first demonstration of SEMPA was made by adding a low resolution scanning electron gun to a Mott spin analyzer.[16] Since then, Koike and co-workers have continued to improve the electron gun until essentially a SEM has been built around a Mott analyzer.[17]

At the National Bureau of Standards, we took a different approach and developed a new spin analyzer which could be easily added to a SEM.[18,19] This analyzer is fist-sized, operates at 150 eV electron beam energy, and is as efficient as the best Mott analyzer. A schematic of such a spin polarization analysis system[20] on an SEM is illustrated in Figure 1. The secondary electrons generated by the scanning primary beam are collected by the extraction optics and transported to the spin polarization analyzer. Each spin analyzer can measure the two polarization components transverse to the electron beam. The third component can be measured by deflecting the beam 90° in the "switchyard" to the second, orthogonal spin analyzer. Thus the direction and magnitude of the polarization vector, and hence the direction and relative magnitude of the magnetization vector, can be completely determined. Spin polarization analyzers lie between secondary electron detectors and Auger energy analyzers in efficiency, so typical magnetization images are intermediate between secondary and Auger images in the time required for accumulation.[21]

Images of Magnetization

Using SEMPA, we have imaged domains in a wide variety of materials including silicon-iron single crystals, permalloy thin film recording head structures, ferromagnetic glasses, Co-Ni recording media, and few-monolayer, epitaxial iron films. SEMPA magnetization images can be obtained from any ferromagnetic or ferrimagnetic material which is sufficiently conductive, or even from an insulator if charging can be overcome.

In the following, we select magnetization images from a few materials to show the salient features of SEMPA:

1. SEMPA can determine each component of the polarization and therefore gives an image of the vector magnetization;
2. the contrast between domains can be very large;
3. the magnetization image is independent of the surface topography unless the topography actually affects the magnetic microstructure;
4. very high spatial resolution can be obtained; and
5. SEMPA is sensitive even to a magnetic film a few monolayers thick.

Magnetization images from a silicon-iron crystal illustrate some of the advantageous features of SEMPA. A regular domain pattern is obtained when the crystal is oriented so that the surface contains the easy axes of magnetization, [100] and [010] for a (001) surface. When the crystal is a few degrees off an easy axis, closure domains result which give the striking "fir tree" pattern.[3] In Figure 2 we show two orthogonal polarization images at relatively low magnification in order to display such a pattern

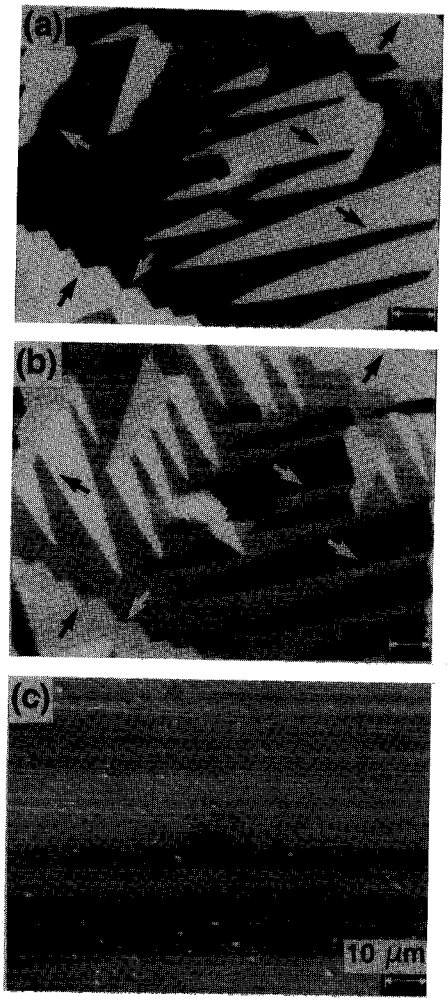

Figure 2. Magnetic domain structure of an Fe-3% Si crystal. The magnetization projected onto the two orthogonal spin analyzer axes is displayed in (a) and (b). Note the complementary nature of the two images and the excellent magnetic contrast. The gray levels give the four different magnetization directions in the domains as marked by the arrows. The intensity image of the same area is shown in (c).

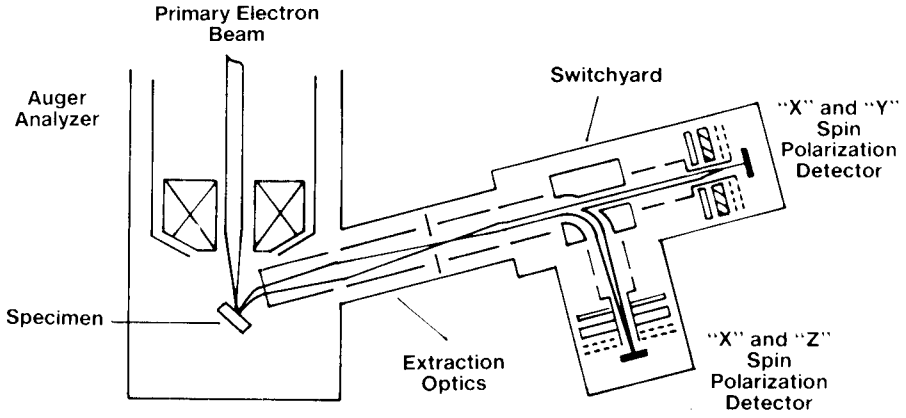

Figure 1. Schematic of a SEMPA apparatus. The secondary electron extraction optics and spin analyzer are added to a UHV SEM/scanning Auger microprobe (from Reference 20).

and the corresponding intensity image for this Fe-3% Si crystal cut off axis. The gray scale in Figure 2a corresponds to the degree of polarization. The arrows indicate direction of magnetization in the domains, which is in the plane of the sample surface. The light and dark areas of Figure 2a appear as intermediate gray levels in Figure 2b, which measures the polarization in an orthogonal direction. (If the axes of the polarization detector were precisely aligned with the crystal easy axes of magnetization, there would be only one intermediate gray level). The measurement completely

determines the polarization vector and hence the direction of magnetization and its relative magnitude. The magnetic contrast as evidenced in Figure 2 is very high. High contrast can be obtained in polarization images without background subtraction. The surface topography of precisely the same area as the magnetization images is displayed in the conventional SEM intensity image of Figure 2c.

Because SEMPA yields topographic and magnetization images simultaneously but independently, it is possible to investigate the effect of surface defects on magnetic microstructure. Images of a Fe-3% Si crystal at somewhat higher magnification are shown in Figure 3. The dagger-shaped domain shown in Figure 3a appears to have domain walls pinned at surface defects pointed out by the arrows in Figure 3b. We are currently coupling SEMPA with a scanning Auger microprobe to allow the investigation of the role of compositional defects or inhomogeneities, in addition to structural defects, on magnetic domain configurations. The resolution apparent from Figure 3 is approximately 100 nm. We have obtained images with a spatial resolution of 50 nm limited only by the electron microscope and expect that resolution better than 10 nm will be possible.

We turn now to magnetization images of other materials. The specimen need not be crystalline, as illustrated by the magnetization and intensity images of a ferromagnetic glass shown in Figures 4a and 4b, respectively. Amorphous ferromagnets can have many useful characteristics, such as low coercivity and losses and high permeability and magnetostrictive coupling. When annealed in a transverse magnetic field, this 40 μm thick $Fe_{80}B_{20}$ metglass ribbon has broad regular domains. Strain, however, can induce an easy axis perpendicular to the surface, causing a complex pattern of closure domains as seen in Figure 4a. Low magnification was used to display this lovely pattern.

Magnetization images can be used to investigate the strain in such specimens.[22] The contrast and definition exhibited in Figure 4a is better than can be obtained by domain imaging with the Bitter technique or magnetic-optic Kerr effect. The broad vertical bands in the topographic image of Figure 4b indicate a wavy surface on that part of the copper wheel where this specimen was quenched. Two large point-like defects visible in the intensity image actually influence the domain configuration as seen in the magnetization image.

Figure 5 shows two orthogonal magnetization images of a 1.5 μm thick permalloy film on a Si substrate in which a boundary in the shape of a recording head (distorted in the image by the tilt in the SEM) has been etched. This magnetically soft, high permeability polycrystalline disordered Fe-Ni alloy has many applications, including magnetic recording. At the edges of the thin film structure are closure domains, three of which are highlighted by arrows in Figures 5a and 5b. An advantage of SEMPA over other domain observation techniques is that both in-plane components of the magnetization can be imaged simultaneously — note how the light closure domains in Figure 5a are dark in Figure 5b, and vice versa.

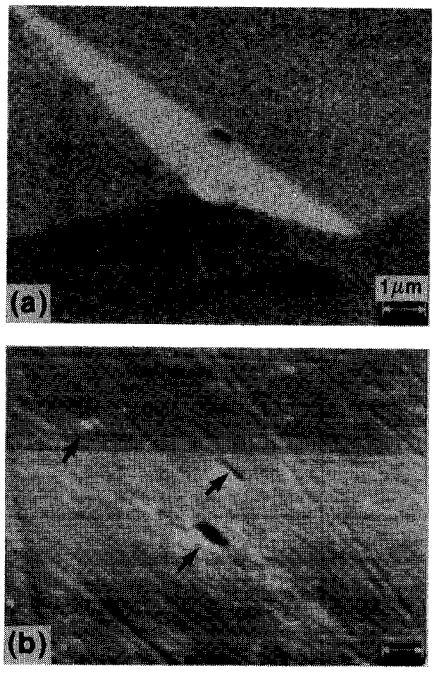

Figure 3. High resolution polarization (a) and intensity (b) images show how the walls separating the three domains in (a) are pinned by the three defects observed in (b).

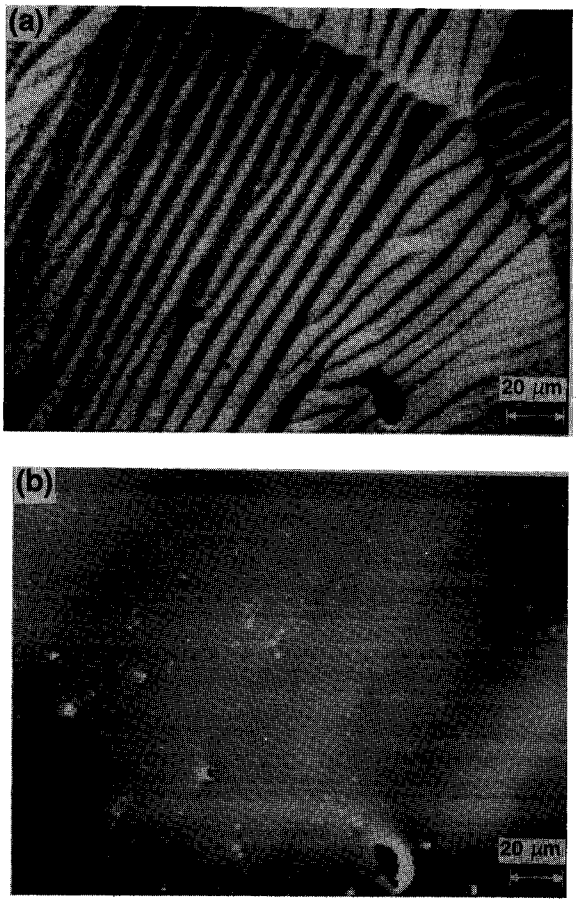

Figure 4. Fine domain structure of an Fe-based metglass shown in (a), with corresponding intensity images in (b).

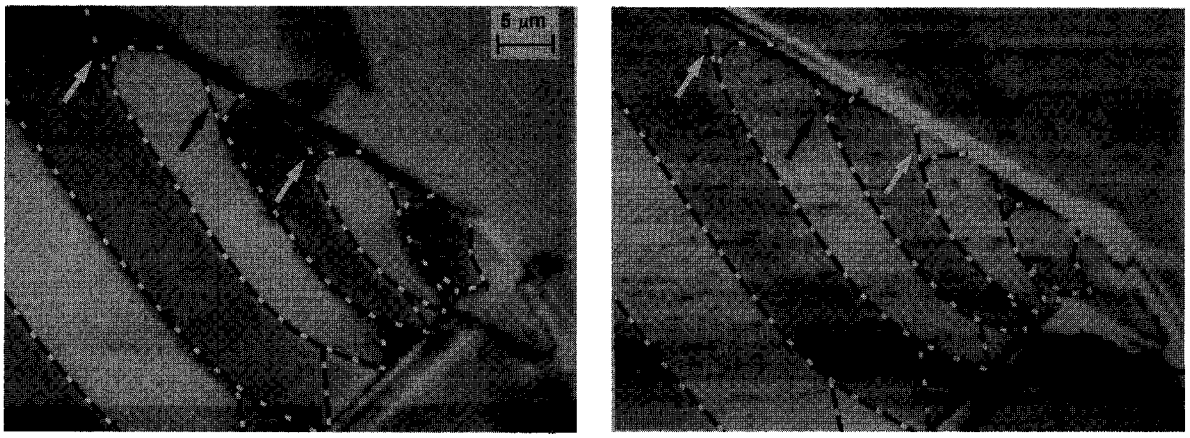

Figure 5. The magnetization image of a permalloy film at an early stage of recording head manufacture. The two orthogonal polarization images, with the domains outlined for clarity, display closure domains along the edge, three of them indicated by the arrows.

Such closure domains are important since they have a different frequency response from the other domains, which decreases head performance. High magnification images (not shown here) allow investigating further domains in the pole tip region which are a source of noise.

All the above examples showed results from specimens ranging in thickness from a few to many micrometers. Because the secondary electrons are emitted from the outer few nanometers of the specimen, SEMPA is also very sensitive to magnetism in thin films. We have observed[23] domains on an Fe film just over three atomic layers thick, ~0.7 nm. As an example of this type of measurement, we show in Figure 6 measurements of a 1.5 nm thick Fe film epitaxially grown in an Ag(100) substrate. It was evaporated through a grid to provide patches approximately 300 μm × 300 μm. The patches were magnetized in plane. A pulsed coil was used to reverse the magnetization. Figure 6 shows the result of subtracting two polarization images of the patches magnetized in two opposite directions. This verifies that the observed effect is truly a magnetic one and rules out the possibility of spurious effects. The line scan shows that the total change in polarization is 55%.

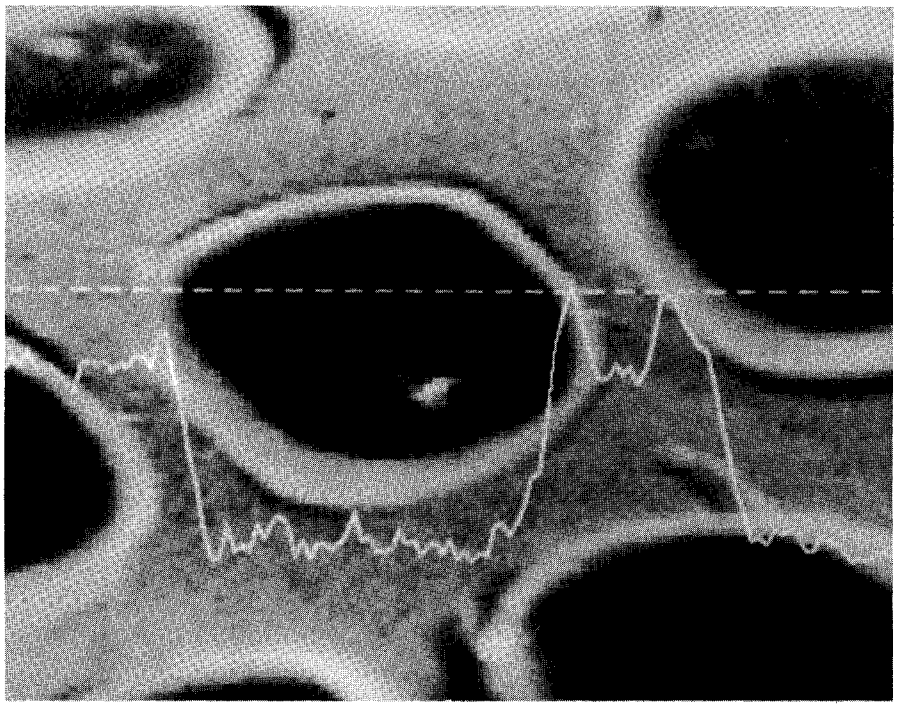

Figure 6. The dark patches on the image represent the change in secondary electron spin polarization on reversal of the thin Fe film magnetization. The light background is the nonmagnetic Ag substrate. The superimposed line scan shows a change in polarization of 55% sampled along the broken line.

Summary

Although SEMPA is a relatively new technique, it is rapidly finding applications to a wide variety of magnetic problems in a wide range of materials. It fulfills the need for a technique that provides high resolution images of each component of the magnetization vector. Specimens can be thick crystals or thin films—there is no need for specimen thinning. It has the power to independently measure and correlate magnetization with topography and, if used with an Auger microprobe, surface chemical composition. Because of the high spatial resolution available in SEMPA, studies of spin rotation in domain walls and of dimensional effects in structures with sizes comparable to domain wall widths will be possible. SEMPA affords the means to study magnetic systems on the scale necessary to meet the demand for higher density recording systems. We expect SEMPA to play an important role in the study of micromagnetism in the future.

Acknowledgments

We wish to acknowledge the collaboration of the Naval Research Laboratory, the Naval Surface Weapons Center, The Universidad Complutense, Madrid, Control Data Corporation, and Eastman Kodak Company in the experiments mentioned. This work was supported in part by the Office of Naval Research.

References

1. P. Weiss, *J. Phys.* **6** (1907) p. 661.
2. F. Bitter, *Phys. Rev.* **38** (1931) p. 1903.
3. H.S. Williams, R.M. Bozorth, and W. Shockley, *Phys. Rev.* **75** (1949) p. 155.
4. D.E. Newbury, D.C. Joy, P. Echlin, C.E. Fiori, and J.I. Goldstein, *Advanced Scanning Electron Microscopy and X-Ray Microanalysis* (Plenum Press, New York, 1986) p. 147.
5. J.P. Jakubovics, in *Electron Microscopy in Materials Science Part IV*, edited by E. Ruedl and U. Valdre (Commission of the European Communities, Brussels, 1973) p. 1305.
6. J. Kranz and A. Hubert, *Z. Angew. Phys.* **15** (1963) p. 220.
7. R. Feder, *Polarized Electrons in Surface Physics* (World Scientific, Singapore, 1985).
8. R.J. Celotta and D.T. Pierce, *Science* **234** (1986) p. 333.
9. J. Unguris, D.T. Pierce, A. Galejs, and R.J. Celotta, *Phys. Rev. Lett.* **49** (1982) p. 72.
10. J. Glazer and E. Tosatti, *Solid State Commun.* **52** (1984) p. 905.
11. D.R. Penn, S.P. Apell and S.M. Girvin, *Phys. Rev. Lett.* **55** (1985) p. 518.
12. E. Kisker, W. Gudat, and K. Schroeder, *Solid State Commun.* **44** (1982) p. 591.
13. H. Hopster, R. Raue, E. Kisker, G. Guntherodt, and M. Campagna, *Phys. Rev. Lett.* **50** (1983) p. 70.
14. R.J. Celotta and D.T. Pierce, in *Microbeam Analysis - 1982*, edited by K.F.J. Heinrich (San Francisco Press, 1982) p. 469.
15. J. Kessler, *Polarized Electrons* (Springer, Berlin, 1985) p. 230.
16. K. Koike and K. Hayakawa, *Jpn. J. Appl. Phys.* **23** (1984) p. L187.
17. K. Koike, H. Matsuyama, and K. Hayakawa, *Scanning Microscopy Supplement* **1** (1987) p. 241.
18. J. Unguris, G.G. Hembree, R.J. Celotta, and D.T. Pierce, *J. Microscopy* **139** (1985) p. RP-1.
19. J. Unguris, D.T. Pierce, and R.J. Celotta, *Rev. Sci. Instrum.* **57** (1986) p. 1314.
20. S.P. Clough and W.J. Eberle, *PHI Interface* **10** (1987) p. 4.
21. G.G. Hembree, J. Unguris, R.J. Celotta, and D.T. Pierce, *Scanning Microscopy Supplement* **1** (1987) p. 229.
22. J.D. Livingston, *J. Appl. Phys.* **57** (1985) p. 3555.
23. J.L. Robbins, R.J. Celotta, J. Unguris, D.T. Pierce, B.T. Jonker, and G.A. Prinz, *Appl. Phys. Lett.* (in press). □